Reversibility of $^1O_2$ Reactions with Acene-doped Conjugated Polymer Nanoparticles and Thin Films

An Honors Thesis for The Department of Chemistry

by

Yimin Zhang

Tufts University

May 2017

I. Introduction

The detection and the quantification of singlet oxygen are very important for understanding its mechanism of action in various chemical, biological, and therapeutic processes. Singlet oxygen ($^1O_2$) detection in water presents a challenge due to the high reactivity and short lifetime of $^1O_2$ in aqueous environments, which makes directly detecting $^1O_2$ by measuring its weak phosphorescence at 1270 nm very difficult.[1] Advances in luminescent probes reported in the literature and commercial singlet oxygen detectors, such as Singlet Oxygen Sensor Green (SOSG, ThermoFisher Scientific) has improved the efficiency of $^1O_2$ detection.[1-3] These probes are often comprised of a two chromophore system. One of the chomophores is a diene (such as an anthracene derivative) that undergoes [4+2] cycloaddition reactions with $^1O_2$ and to form an endoperoxide and slow the rate of photoinduced electron transfer between an excited state of a coupled chromophore (such as a fluorescein in SOSG) and the anthracene.[4-7] The resulting disruption of the energy transfer pathway yields an increased quantum yield of luminescence of the non-anthracene chromophore. A wide variety of acenes with highly tunable emission wavelengths and $^1O_2$ reactivity rates can be used instead of anthracene as the diene in a $^1O_2$ probe. However, the hydrophobic nature of the chromophores used in these $^1O_2$ detectors still poses a challenge when detecting $^1O_2$ in water.

Previously the Thomas group demonstrated a ratiometric fluorescence response to $^1O_2$ in organic solvent using acene-linked conjugated polymers comprised of a poly(phenylene-co-fluorene) backbone and a $^1O_2$-reactive linear acene bound via an insulating four-carbon linker.[8] A comparable system in water using diarylacene methacrylate pendants on water-soluble (oligoethylene glycol) methacrylate (OEGMA)-based polymers harnesses the $^1O_2$ detection capabilities of acenes for use in aqueous environments, but the low chromophore density of these

acene-OEGMA copolymers slows energy transfer and limits the range of ratiometric responses available.[9] Acene doped conjugated polymer nanoparticles take advantage of the ratiometric fluorescence response displayed by acene-linked conjugated polymers in organic solvent and the hydrophobic nature of both the acene and the conjugated polymer to form nanoparticles in an aqueous environment.

The cycloreversion of the endoperoxides formed by alkynyl-substituted acenes in organic solvent has been well-documented.[10] The aim of the research described in this thesis is to report the cycloreversion of the endoperoxide of 9,10-bis((4-methoxy-phenyl)ethynyl)anthracene (DE-ANT) when doped in poly(9,9-di-*n*-octylfluorenyl-2,7-diyl) (PFO, a fluorescent conjugated polymer) nanoparticles in water and the extent to which this cycloreversion can undergo continuous cycles of irradiation and heating at various acene doping percentages. We also seek to answer the following four fundamental questions:

1. How does acene doping percentage affect the initial spectrum of DE-ANT/PFO nanoparticles?
2. How does acene doping percentage affect the fluorescence spectra during irradiation?
3. What is the effect of heat as a function of time?
4. How does the doping percentage affect how the nanoparticles perform during continuous cycles of irradiation and heating?

The endoperoxide of DE-ANT was chosen specifically because it reconverts to the parent acene and singlet oxygen faster than the endoperoxides of other substituted acenes and heteroacenes previously reported by the Thomas group. There is also a large spectral overlap between the absorbance of DE-ANT and the emission PFO which results in highly efficient

fluorescence resonance energy transfer (FRET) and makes DE-ANT the ideal acene for doping into PFO nanoparticles. However, the fluorescence emission ratio of the PFO to the PFO plus DE-ANT in the nanoparticles never returns to its initial ratio. This suggests that full reversion of the endoperoxide to the parent acene is not occurring, so DE-ANT was doped into optically clear poly(methyl methacrylate) (PMMA) thin films to mimic the solid nanoparticle matrix, while simplifying the system to one chromophore.

II. Background

Conjugated polymers are rigid rod-like polymers due to the rigidity of the π-conjugated backbone.[13] The delocalized pi system resulting from the sp^2 confirmation of each carbon in the backbone promotes electron mobility. Conjugated polymer nanoparticles have been shown to have biosensing and fluorescence imaging applications.[12,18] Compared to similarly sized metal nanoparticles and inorganic quantum dots, they are easily prepared via precipitation in water. Conjugated polymer nanoparticles are also very bright, photostable, have low cytotoxicity, and high cellular uptake.[12]

A. Acenes

Acenes are a class of polycyclic aromatic hydrocarbons characterized by their linearly fused benzene rings. The optical properties and $^1O_2$ reactivity of acenes can be tuned by varying the number of linearly fused benzene or thiophene rings along their long axes and varying arylethynyl substituents along the short acene axes.[11] Diethynyl substitutions lower the activation energy of endoperoxide cycloreversion by stabilizing the carbon radical intermediate.[19] Diethynyl substitutions also enhances the oxidation stability of acenes and protects the resulting

endoperoxides from thermal decomposition.[10,11,19] Adding a benzene ring to the long axis decreases the HOMO−LUMO gap, while adding a terminally fused thiophene ring decreases the HOMO−LUMO gap by 50−60% of the decrease in HOMO−LUMO gap that results from the addition of a benzene ring.[11]

Considering these properties, DE-ANT, DE-AMT, and DE-TET were chosen as potential acenes to be doped into conjugated polymer nanoparticles and tested for cycloreversion. DE-ANT is an anthracene derivative, so it should react the slowest with $^1O_2$ due to its large HOMO-LUMO gap, while DE-TET, a tetracene derivative should react the fastest because of its small HOMO-LUMO gap, while the terminal thiophene ring on DE-AMT should cause it to react with $^1O_2$ at a rate in between that of DE-ANT and DE-TET. [10,11] However, the reverse reaction for DE-ANT should be significantly faster than that of DE-AMT and DE-TET.[10,11] Each acene was paired with a conjugated polymer whose emission spectra had a large spectral overlap with the absorbance of the acene to increase fluorescence resonance energy transfer (FRET) efficiency. So DE-ANT and DE-AMT were doped into PFO nanoparticles, while DE-TET was doped into PFPV.[11,12]

B. Singlet Oxygen

Singlet oxygen is a high-energy form of molecular oxygen that is a natural byproduct of oxidative phosphorylation in mitochondria and chlorophyll-driven photosynthesis in plants.[14] In high concentrations, singlet oxygen, like other reactive oxygen species, is capable of damaging DNA, oxidizing polyunsaturated fatty acids in lipids, amino acids in proteins, and co-factors leading to the oxidative deactivation of specific enzymes.[14] Singlet oxygen is significantly more electrophilic than oxygen in its normal energy state and will thus readily react with any biomolecule by oxidizing phenols, unsaturated carbon-carbon bonds, neutral nucleophiles such

as sulfides and amines, and it will even react with anions.[1] If enough of these damages occur, the cell undergoes apoptosis.

Under normal physiological conditions, the intracellular levels of reactive oxygen species are kept in check by non-enzymatic molecules (i.e. glutathione, flavenoids and vitamins A, C and E) or through antioxidant enzymes to prevent cells from damage.[1] However these detoxification mechanisms are often not steadily maintained in cancer cells have been shown to produce increased levels of singlet oxygen and other reactive oxygen species due to their increased metabolic rate. Thus, detecting increased singlet oxygen levels can be used to detect tumor cells.

Meanwhile, neutrophils and macrophages produce reactive oxygen species to kill tumor cells, so high levels of artificially generated singlet oxygen have the potential to be used in the treatment of tumors. The cytotoxicity of singlet oxygen makes it particularly useful in photodynamic therapies. During photodynamic therapy, photosensitizers are activated using light once an appropriate quantity has accumulated in the target cells. These sensitizers then generate singlet oxygen and other reactive oxygen species which wreak havoc on various biomolecules.

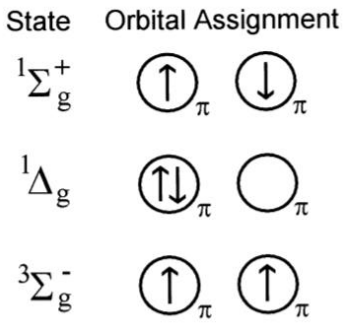

Figure 1. Representations of the π antibonding molecular orbitals of molecular oxygen O_2: $^1\Delta_g$ singlet oxygen and $^1\Sigma^+_g$ singlet oxygen, and $^3\Sigma^-_g$ triplet oxygen.[1]

The two lowest singlet oxygen states and the triplet state of molecular oxygen are shown in Figure 1. Molecular oxygen O_2 typically exists in the $^3\Sigma^-_g$ triplet state and can be excited to

the singlet oxygen state by visible light. The $^1\Delta_g$ singlet oxygen is relatively long-lived due to the spin forbidden transition from the $^1\Delta_g$ singlet oxygen state to the $^3\Sigma^-_g$ triplet oxygen state, but the $^1\Sigma^+_g$ singlet oxygen state is relatively short-lived in both the gas phase and in solution due to the spin-allowed transition from the $^1\Sigma^+_g$ state to the $^1\Delta_g$ state.[1] Despite the spin forbidden transition, laser spectroscopy can be used to directly detect the weak phosphorescence of the $^1\Delta_g$ singlet oxygen transition to $^3\Sigma^-_g$ triplet oxygen at 1270 nm.[1] However, this detection method is not practical in biological systems due to the weak signal produced by this transition and singlet oxygen's short lifetime of just under a second, so photochemists have proposed using a variety of fluorophores that react with singlet oxygen to extend the detection time of singlet oxygen. Thus, the rate of singlet oxygen generation can be indirectly measured by measuring the change in absorbance or fluorescence of various fluorophores such as 1,3-diphenylisobenzofuran (DPBF) or 9,10-anthracenediyl-bis (methylene) dimalonic acid (ABDA) which react with singlet oxygen to become endoperoxides.

C. Photosensitizers

In photochemistry, singlet oxygen is traditionally generated using a photosensitizer such as methylene blue (Fig. 2A.) or rose Bengal (Fig. 2B.) that excites the triplet energy state of molecular oxygen to singlet oxygen when exposed to a wavelength light absorbed by the photosensitizer.[1] The large de-located π systems found in most photosensitizers lower the energy of highest occupied molecular orbitals (HOMO) and its absorbance of light sometimes ionizes the molecule. The ideal photosensitizer has a strong absorbance in the red/near infrared region of the electromagnetic spectrum (600-850 nm), high singlet oxygen quantum yield, and low cytotoxicity in the dark.

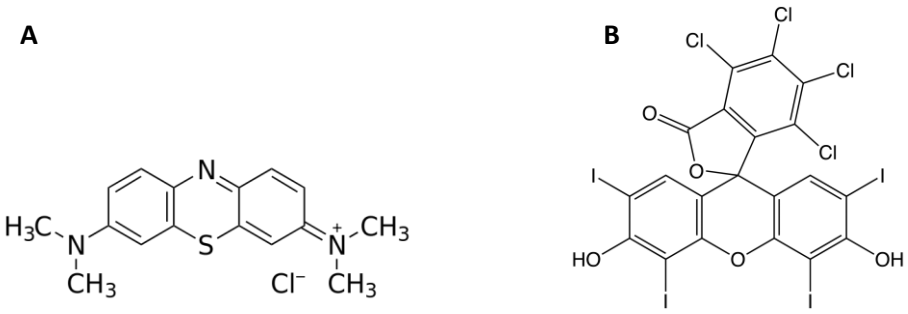

Figure 2. A) Methylene blue and B) Rose Bengal

The two ways in which molecular oxygen can react with a photosensitizer are defined as Type I and II mechanisms. The Type I mechanism involves either hydrogen-atom abstraction or electron-transfer between an excited photosensitizer and a substrate.[1] This generates substrate free radicals which then react with oxygen to form a cascade of active oxygen species, starting with the high-energy superoxide radical anion (O_2•−), which goes on to produce the highly reactive hydroxyl radical (OH•), eventually leading to singlet oxygen generation.[1] The Type II mechanism, the excited sensitizer collides into triplet oxygen and the resulting energy transfer produces singlet oxygen.[1]

The PFO nanoparticles used in the acene-doped nanoparticle system are negatively charged, so positively charged external photosensitizers such as methylene blue and rose Bengal coat the outside of the nanoparticle and interfere with the cycloaddition and cycloreversion of $^1O_2$ with the nanoparticles.[18] So instead of using an external photosensitizer, the acene DE-ANT will act as a self-sensitizer to mimic the conditions these nanoparticles would be used in a biological system. Figure 3 shows the excited acene entering the triplet state upon irradiation with visible light and self-sensitize $^1O_2$ via the Type II mechanism. The excited conjugated polymer will transfer energy to the acene via what we hypothesize to be the Förster mechanism

to generate more $^1O_2$. The $^1O_2$ generated, then undergoes [4+2] cycloaddition with the acene to form an endoperoxide.

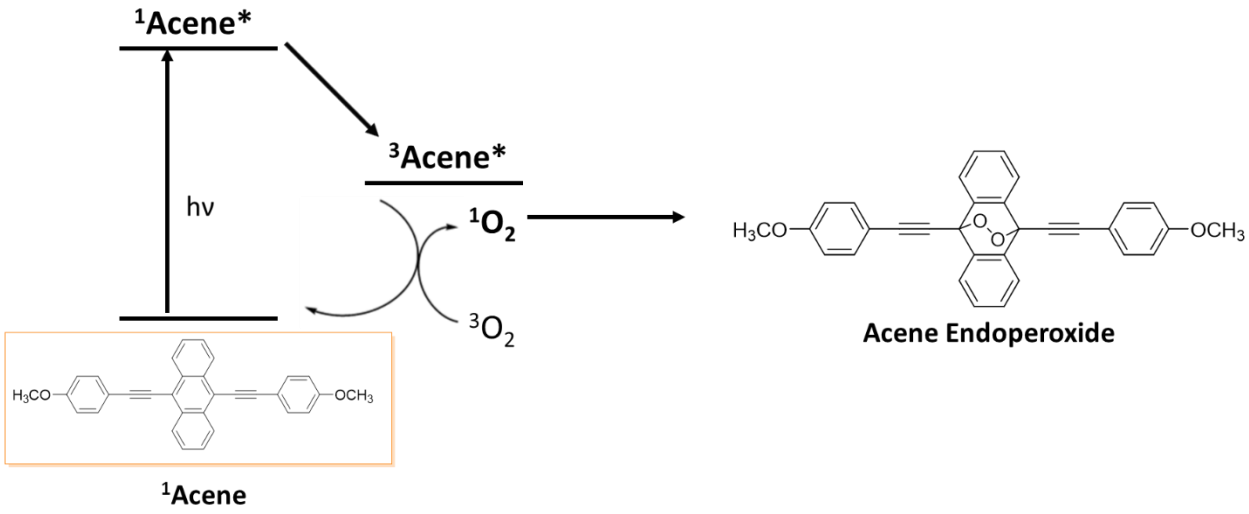

Figure 3. $^1O_2$ sensitization and cycloaddition with acenes using acenes as the photosensitizer.

III. Experimental Methods

General Considerations: All chemicals were purchased and received from commercial sources and used without further purification. Dry solvent was obtained from Innovative Technologies PureSolv 400 solvent purifier. Silica gel (230-400 mesh) was used as the stationary phase for flash chromatography.

^{1}H NMR spectra were obtained on a Bruker DPK-300 or Bruker Avance III 500 spectrometer and can be viewed in Supporting Information. Chemical shifts are reported relative to $CHCl_3$ (7.26 ppm).

A. Materials and synthetic methods

9,10-Bis((4-methoxy-phenyl)ethynyl)anthracene (DE-ANT). The synthesis procedure outlined by *Fudickar and Linker* was followed except with the following modifications.[10] 9,10-dibromoanthracene (212 mg, 0.63 mmol), $[Pd(PPh_3)_2Cl_2]$ (37.6 mg, 0.05 mmol) and CuI (63.4 mg, 0.33 mmol) were placed in a two-necked 25 ml round bottom flask along with a magnetic stir bar and a condenser and sealed with a septum before being dissolved in dry THF (8 mL) and dry iPr_2NH (8 mL). Argon was bubbled through the reaction mixture to eliminate O_2. The reaction was then heated to 80°C. At 80°C 4-methoxyphenylacetylene (1.3 mmol) was added neat via syringe over a period of 1.5 h. Allowed Sonogashira reaction to heat overnight. A TLC was done on the reaction product using 40% CH_2Cl_2/hexanes to make sure the reaction had run to completion. The reaction product was transferred to a 250 ml round bottom flask with CH_2Cl_2 and concentrated. The reaction product was then purified via flash chromotography (40% CH_2Cl_2/hexanes). Based on TLC and the ^{1}H NMR spectra of the fractions, fractions 9-19 were recrystallized using a mixture of CH_2Cl_2 and hexanes.

Yield 57.8 mg (20.9%), orange crystals. ^{1}H NMR (300 MHz, $CDCl_3$): δ=3.88 (6H, s, OMe), 6.98 (4H, d, *J*=8.6 Hz, ArH-3, ArH-5), 7.61 (4H, dd, *J*=3.1 Hz, 6.6 Hz, H-2, H-3, H-6, H-7), 7.71 (d, *J*=8.6 Hz, ArH-2, ArH-6), 8.67 (4H, dd, *J*=3.1 Hz, 6.6 Hz, H-1, H-4, H-5, H-8).

Scheme 1. Synthesis of 9,10-Bis((4-methoxy-phenyl)ethynyl)anthracene (**DE-ANT**)

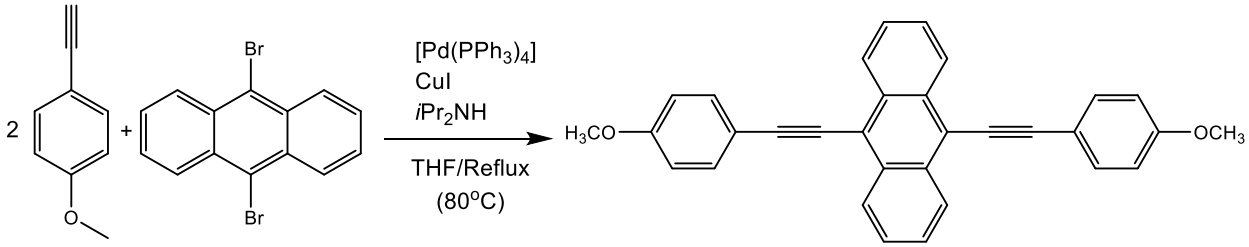

B. Doping nanoparticles with acene

The conjugated polymer poly(9,9-di-*n*-octylfluorenyl-2,7-diyl) (PFO, MW 40,000 - 150,000) was purchased from ADS Dyes, Inc. (Quebec, Canada). The solvent tetrahydrofuran (THF) was purchased from Sigma-Aldrich (Milwaukee, WI). Stock solutions of PFO (10 mg in 5 ml of THF) and DE-ANT (10 mg in 5 ml THF) were dissolved by sonication for 30 min and then filtered through a 0.2 μm polytetrafluoroethylene (PTFE) syringe filter to remove any insoluble material. 100 ppm DE-ANT/PFO in THF solutions were prepared in various doping weight percentages. For nanoparticle preparation, DE-ANT/PFO nanoparticles were prepared by injecting each DE-ANT/PFO in THF solution (1 ml of 100 ppm) into 10 ml of water respectively under ultra-sonication followed by 15 additional seconds of ultra-sonication. Two samples of each acene doping percentage were prepared. The THF was removed using rotary evaporation, and a small fraction of aggregates was removed via filtration through a 0.2 μm PTFE filter. The resultant nanoparticle solutions ranged from light green to clear under room light and blue-green under UV light.

C. Optical Measurements

All optical measurements of nanoparticles and thin films were performed in air at ambient temperature and humidity. UV-vis absorbance, fluorescence emission and excitation spectra were taken to characterize the nanoparticles and thin films using parameters outlined in the Results and Discussion. The size distribution of the nanoparticles was determined using dynamic light scattering (DLS, Malvern Zetasizer Nano-ZS). The fluorescence intensity of nanoparticle solutions and thin films was determined using a fluorimeter (PTI Quantum Master 4 equipped with a 75 W Xe lamp), and the absorbance spectrum was obtained with UV-vis spectroscopy (Varian Cary-100, double-beam mode using a solvent-containing polymethacrylate cuvette or glass cover slip for background subtraction spectra). All fluorescence spectra were corrected for the output of the lamp and the dependence of detector response to the wavelength of emitted light. Irradiation for production of singlet oxygen was performed with a 200W Hg/Xe lamp (Newport-Oriel) equipped with a manual shutter and a FSQ-BG40 blue bandpass filter. Focused light was used to irradiate the nanoparticles and unfocused light was used to irradiate the thin films.

IV. Results and Discussion

The objective of this work was to determine the reversibility of $^1O_2$ reactions with acene-doped conjugated polymer nanoparticles. These nanoparticles display a large acene fluorescence emission and a small conjugated polymer emission when first assembled, but upon irradiation, the acene emission decreased and the conjugated polymer emission increased. This process can then be reversed by heating the nanoparticles to 80°C.

A large amount of work done was to optimize the nanoparticle system. DE-ANT, DE-AMT, and DE-TET were tested as potential acenes. DE-ANT was found to be slightly less photosensitive than DE-AMT and significantly less than DE-TET which makes it the ideal candidate for successive cycles of irradiation and heating. Attempts to optimize DE-AMT using PFO and poly(2,5-di(3′,7′-dimethyloctyl)phenylene-1,4-ethynylene) (PPE) polymers were unsuccessful. Direct irradiation of DE-TET/PFPV nanoparticles photobleached both DE-TET and PFPV. So DE-ANT was ultimately chosen as the acene because the cycloreversion of DE-ANT has been well-documented, but the extent to which it can be pushed is not known.[10] [YZ1]

A. Effect of different precipitation ratios on nanoparticle size

Wu et. al. previously reported that higher precursor polymer concentrations resulted in larger nanoparticle sizes and that 2 ml of 20 ppm conjugated polymer in THF solution to 8 ml of water produced nanoparticles of ~50 nm. However, preliminary experiments conducted for this thesis using poly(9,9-di-*n*-octylfluorenyl-2,7-diyl) (PFO, MW 20,000) purchased from Sigma-Aldrich (Milwaukee, WI) consistently showed this precipitation ratio produced nanoparticles that were either too large to be efficiently filtered through a 0.2 µm polytetrafluoroethylene (PTFE) syringe filter or too polydisperse for DLS size measurements to be taken. So in an effort to

decrease nanoparticle size, 20 ppm and 100 ppm PFO/THF solutions were precipitated in various ratios of polymer in THF solution to water (See Table 1 and 2). Precipitation causes a sudden decrease in solution hydrophobicity and triggers a competition between aggregation and chain collapse to form nanoparticles.[12] Since acenes are hydrophobic fluorescent dyes so they can be easily incorporated into PFO nanoparticles by including them in the precursor solution before precipitation.

Table 1. Size distribution of 20 ppm PFO nanoparticles.

Sample Content	**Z-Ave (d nm)**	**PDI**	**Comments**
2 ml of 20 ppm PFO in 8 ml Millipore water	High PD	__	Could not optimize, too polydisperse for DLS to measure
1 ml of 20 ppm PFO in 9 ml Millipore water	76	0.07	6 drops of sample, good Correlation Function, however 2A.2 was polydisperse
1 ml of 20 ppm PFO in 10 ml Millipore water	85	0.15	6 drops of sample, good Correlation Function, however 3A.2 was polydisperse
2 ml of 20 ppm PFO in 10 ml Millipore water	133	0.22	6 drops of sample, good Correlation Function, howeve 4A.1 was polydisperse

Table 2. Size distribution of 100 ppm PFO nanoparticles. N=2 for all nanoparticles with reported standard deviation.

Sample Content	**Z-Ave (d nm)**	**PDI**	**Comments**
2 ml of 100 ppm PFO in 8 ml Millipore water	168	0.22	1 ml pure sample, bad Correlation Function, noisy, low count rate ~30k, polydisperse
1 ml of 100 ppm PFO in 9 ml Millipore water	73 ± 6	0.12 ± 0.05	1 ml pure sample, beautiful Correlation Function
1 ml of 100 ppm PFO in 10 ml Millipore water	68 ± 3	0.07 ± 0.04	1 ml pure sample, beautiful Correlation Function
2 ml of 100 ppm PFO in 10 ml Millipore water	116 ± 10	0.05 ± 0.01	1 ml pure sample, beautiful Correlation Function

Based on the data in Tables 1 and 2, nanoparticle size can be controlled by adjusting the polymer concentration in the precursor solution and the precipitation ratio of the polymer/THF solution to water. 1 ml of 100 ppm PFO in 10 ml Millipore water yielded the smallest nanoparticles as measured by z-average. Thus, all future nanoparticles were made using this polymer concentration and precipitation ratio.

B. Effect of different acene doping percentages on cycloreversion

For nanoparticle preparation, stock solutions of DE-ANT (prepared as reported in Experimental Methods) and PFO were prepared in THF and diluted to the concentrations described in the table below to yield 100 ppm DE-ANT/PFO in THF solutions. Acene doping percentage is preserved when these solutions are precipitated in water using the procedure reported in Experimental Methods.

Recipes for preparing nanoparticles:

% DE-ANT/PFO	**1%**	**5%**	**10%**	**20%**
DE-ANT	0.001 mg/ml	0.005 mg/ml	0.01 mg/ml	0.02 mg/ml
PFO	0.099 mg/ml	0.095 mg/ml	0.09 mg/ml	0.08 mg/ml

Each sample was diluted to yield an absorbance of 0.1 at 400 nm. UV-vis absorbance was measured from 290-800 nm. Fluorescence emission spectra were measured using an excitation wavelength of 400 nm, the maximum of the absorbance spectrum and the excitation spectrum was monitored at 492 nm, the maximum of the emission spectrum. Figure 4 shows the UV-vis absorbance and fluorescence spectra of 1%, 5%, 10%, and 20% DE-ANT/PFO nanoparticles. The absorbance spectrum (blue line) contains a peak at 390 nm that is characteristic of α-phase of PFO and peaks at 400 nm and 435 nm characteristic of β-phase PFO.[12] DE-ANT peaks are not seen in the 1% DE-ANT/PFO doping absorbance due to the low percentage of DE-ANT in

relation to PFO. Starting at 5% doping and becoming more prominent in the 10% and 20%, a small shoulder can be seen at 492 nm in the absorbance that is attributed to DE-ANT. The emission spectra are dominated by the intensity of the DE-ANT acene at 492 nm, but a small PFO peak at 441 nm can be seen at all doping levels, so the emission spectra were used to track nanoparticle behavior during continuous cycles of irradiation and heating. The peak at 617 nm in the 20% nanoparticles emission spectrum is most likely due to aggregation that resulted from the high acene concentration.

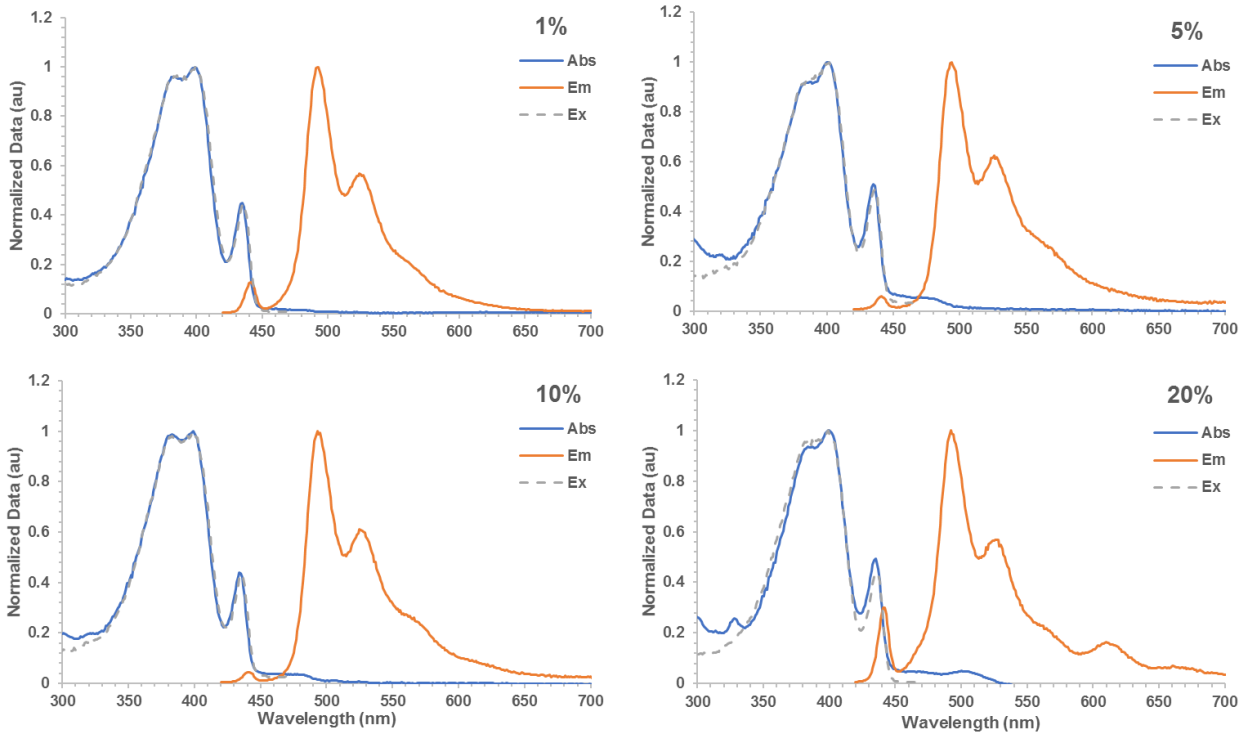

Figure 4. Normalized UV-vis absorbance (left, blue), excitation (left, gray), and emission (right, orange) of DE-ANT/PFO nanoparticles in water.

The nanoparticles were irradiated using a Hg/Xe lamp with focused 300 to 700 nm light (FSQ-BG40 filter) and a power density of 23 mW/cm^2 until the fluorescence intensity of DE-ANT relative to PFO plus DE-ANT has reached a plateau. Figure 5 shows our approach to $^1O_2$ generation and cycloreversion using the acene-doped conjugated polymer nanoparticles. Endoperoxide generation and cycloreversion were tracked by calculating the donor/(donor+acceptor) ratio in the fluorescence emission. PFO is highly photostable and acts as an internal standard for the emission of the nanoparticles.

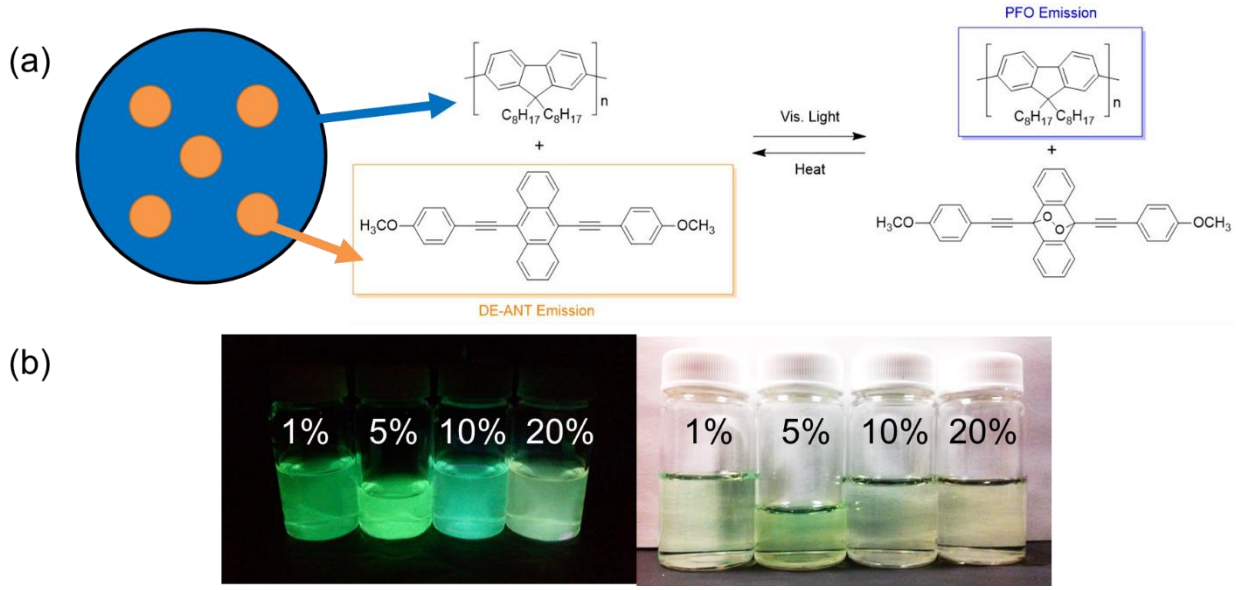

Figure 5. (a) Experimental approach to determining $^1O_2$ generation. Irradiation with visible light generates $^1O_2$, which reacts with the DE-ANT in the nanoparticles. (b) photographs of aqueous nanoparticles under UV light (left) and room light (left).

We theorized that by irradiating the nanoparticles with light absorbed by both the PFO (donor) and DE-ANT (acene) in the presence of molecular O_2, $^1O_2$ is generated. Irradiation will excite both the acene and the conjugated polymer will also be excited. The excited acene will enter the triplet state upon irradiation with visible light and self-sensitize $^1O_2$ via the Type II mechanism. The excited conjugated polymer will transfer energy to the acene via what we

hypothesize to be the Förster mechanism to generate more $^1O_2$. The $^1O_2$ generated, then undergoes [4+2] cycloaddition with the acene to form an endoperoxide. The endoperoxide formation shuts down the energy transfer pathway from PFO to DE-ANT.[8] During the irradiation process, a ratiometric fluorescence response occurs as DE-ANT emission decreases and PFO emission increases in relation to time and results in the PFO emission being dominant at the end of irradiation, thus increasing the donor/(donor+acceptor) ratio (see Supporting Information).[8] Each nanoparticle solution was then transferred to a 3-ml scintillation vial, wrapped in tin foil to block further irradiation, and heated to 80°C in an oil bath. Heating the nanoparticles resulted in a decrease in the donor/(donor+acceptor) ratio by reverting endoperoxide to increase DE-ANT emission, restoring the energy transfer pathway and decreasing PFO emission.

1%, 5%, 10%, and 20% DE-ANT/PFO nanoparticles had initial donor/(donor+acceptor) ratios of 0.12±0.00, 0.059±0.001, 0.054±0.003, and 0.32±0.014 respectively (Figure 6 and 7). Aggregation and acene to acene quenching may have decreased DE-ANT emission contributing to the high initial donor/(donor+acceptor) ratio in the 20% nanoparticles. Our hypothesis was that a lower ratio suggests more efficient energy transfer from the polymer to the acene occurs via the Förster mechanism, which would aid in the cycloreversion of the endoperoxide to the parent acene. Acene reversion occurred in 5%, 10%, and surprisingly 20% DE-ANT/PFO nanoparticles, but 1% DE-ANT/PFO nanoparticles did not revert despite its low initial donor/(donor+acceptor) ratio. $^1O_2$ may be quenched or trapped in the nanoparticle matrix before it can diffuse out of the 1% nanoparticles, which could explain why cycloreversion did not occur.

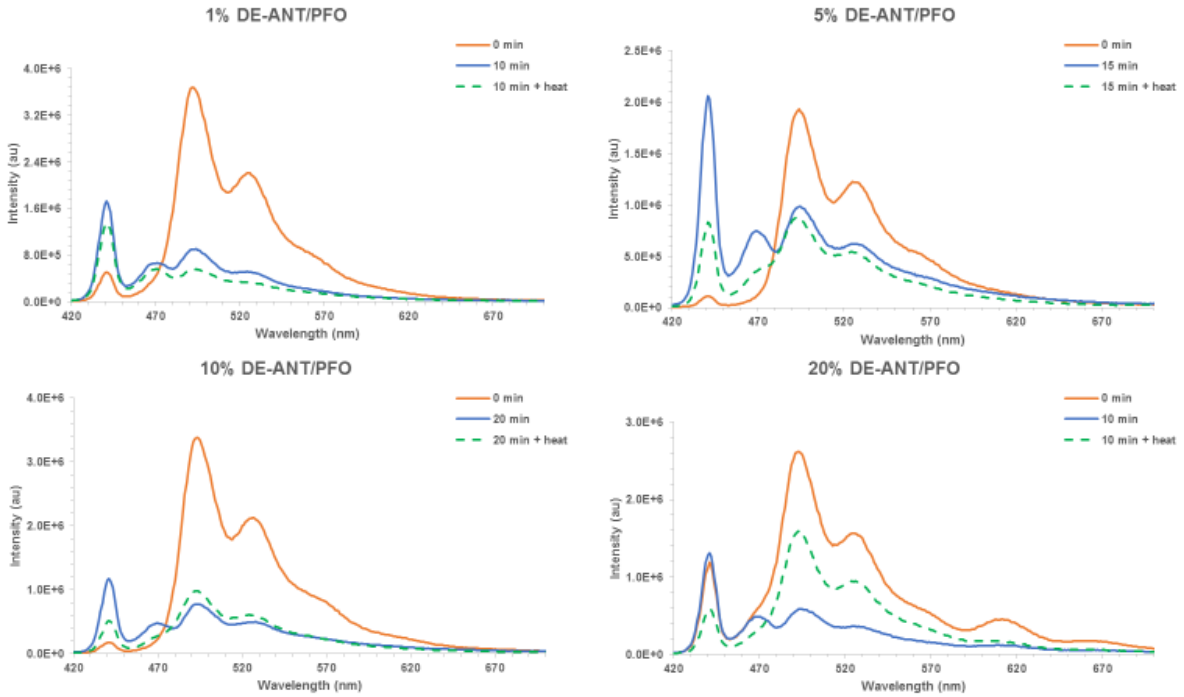

Figure 6. Emission spectra of 1%, 5%, 10%, and 20% DE-ANT/PFO nanoparticles before irradiation (orange line), at the end of irradiation (blue line), and after heating for 1 day (green dashed line).

DLS measurements show the nanoparticles increasing in size at the end of each irradiation and then decreasing in size after heating (Table 3). This suggests that singlet oxygen is being incorporated into the nanoparticle matrix during irradiation to increase nanoparticle z-average. After heating, singlet oxygen has diffused out of the nanoparticle, which decreases the nanoparticle z-average.

Table 3. Nanoparticle Size as measured by the Z-ave (d nm)

ANT/PFO	Initial	After Heat Stabilization (23 hr)	End of First Irradiation	After First Heating (65.83 hr)
1%	53	54	150	90
5%	75	79	122	96
10%	55	76	205	287
20%	98	162	150	122

A preliminary control experiment conducted on 10% DE-ANT/PFO nanoparticles using lower molecular weight PFO from Sigma Aldrich showed that heating the nanoparticles to 80°C increases the donor/(donor+acceptor) ratio from 0.11 until the ratio stabilizes after one day of heating at 0.42±0.01 and remains at this intensity during prolonged heating over time (see SI). This increase in the donor/(donor+acceptor) ratio can be attributed to PFO annealing that occurs at high temperatures.[16] Thermal annealing leads to the formation of γ-phase domains, which consists of a combination of α and β-phase PFO.[16] In the UV-vis absorbance spectra of the nanoparticles after heating, the PFO peak at 390 nm characteristic of α-phase PFO becomes the maximum after heating, which provides further evidence of γ-phase formation after heating (see SI).

To account for the effect of thermal annealing on nanoparticle cycloreversion, 1%, 5%, 10%, and 20% DE-ANT/PFO nanoparticles were heated for 1 day for heat stabilization before undergoing cycles of irradiation and heating. As shown in Figure 7, heat stabilization increased the donor/(donor+acceptor) ratio for 1%, 5%, and 10% nanoparticles, while the ratio for 20% nanoparticles were decreased. Heat-stabilization and the γ-phase formation that resulted broke up the aggregation seen in the 20% nanoparticles. This is further evidenced by a decrease in the at 617 nm in the emission spectra of 20% nanoparticles that we have attributed to aggregation (see SI).

After heat stabilization, 1%, 5%, 10%, and 20% DE-ANT/PFO nanoparticles were all irradiated until the donor/(donor+acceptor) ratio was 0.52±0.02 (Figure 7). Nanoparticles doped at 10% w/w responded the slowest requiring 20 minutes of irradiation, while those doped at 1% and 20% the fastest at 10 minutes. The nanoparticles were then heated to revert the endoperoxide back to the parent acene DE-ANT. 5%, 10%, and 20% DE-ANT/PFO nanoparticles can undergo

multiple cycles of irradiation and heating with minimal photo fatigue evidenced by an overall decrease in nanoparticle emission occurring over time (Figure 7).

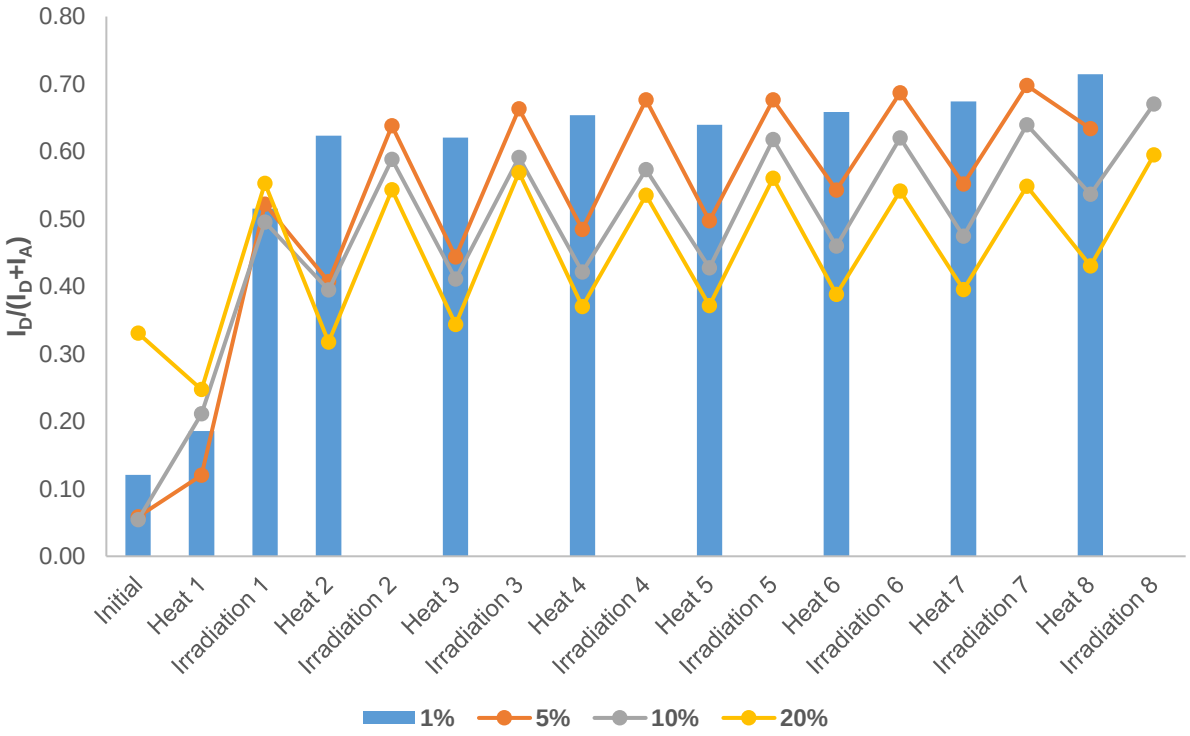

Figure 7. Donor/(donor+acceptor) ratios of heat-stabilized 1%, 5%, 10%, and 20% DE-ANT/PFO nanoparticles during repeated cycles of irradiation and heating (see SI for raw data).

However, acene reversion in 5%, 10%, and 20% DE-ANT/PFO nanoparticles never returns to the initial donor/(donor+acceptor) ratio or even the ratio after heat stabilization. Endoperoxides revert along a stepwise path with radical intermediates.[10,19] Alkyl substituted acenes favor O-O bond cleavage to form radical intermediates followed by decomposition.[19] Aryl and alkynyl substituted anthracenes like DE-ANT favor C-O bond cleavage to form a carbon radical that undergoes rearrangement to yield the parent acene.[19] The lack of full acene reversion in DE-ANT/PFO nanoparticles can be explained by a small fraction of DE-ANT undergoing the decomposition pathway during each heating.

C. Reversion in acene-doped poly(methyl methacrylate) (PMMA) thin films

To simplify the nanoparticle system, DE-ANT was doped in an optically clear poly(methyl methacrylate) (PMMA) thin film to monitor the behavior of acenes trapped in a solid matrix like that of a nanoparticle, but without the interference from the optical and thermal properties of PFO. To understand the implications of the cycloreversion to the acenes and $^1O_2$ on energy transfer, we investigated the optical spectra of the photoproducts resulting from direct irradiation of DE-ANT under atmospheric O_2.

For film preparation, a solution of DE-ANT (prepared as reported in Experimental Methods) and PMMA was prepared in chloroform as described in the table below. Chloroform was used as a solvent instead of THF, as in the nanoparticles, to avoid any effect the BHT inhibitor present in the THF might have on the optical properties of the thin films. Spin-casting (Laurell WS-400-6NPP) onto acetone-cleaned glass microscope cover slips yielded the films.

Recipes for preparing spun-cast thin films:

% DE-ANT/PMMA	**5%**	**10%**	**20%**
DE-ANT	1.3 mg	2.5 mg	5 mg
PMMA	25 mg	25 mg	25 mg
$CHCl_3$	10 ml	10 ml	10 ml
Spin speed	1000 rpm (60 sec)	500 rpm (60 sec) 1000 rpm (60 sec)	500 rpm (60 sec) 1000 rpm (60 sec)

The 5% and 10% DE-ANT/PMMA thin films were a uniform yellow color, but the 20% thin films had localized spots of orange that were most likely areas of DE-ANT aggregation. The emission spectra of the 20% thin films confirmed this observation. Due to the non-uniformity of the 20% thin films, only preliminary spectra that consisted of one round of irradiation and heating was conducted.

The UV-vis absorbance, fluorescence emission and excitation spectra were taken to characterize the thin films (Figure 8). UV-vis absorbance was measured from 200-800 nm. Fluorescence emission spectra were measured using an excitation wavelength of 420 nm and the excitation spectra were monitored at 620 nm. Thin films were irradiated using a Hg/Xe lamp with unfocused 300 to 700 nm light (FSQ-BG40 filter) and a power density of 17.9 mW/cm^2 until the absorbance of the acene peak reached a plateau.

PMMA is an optically clear polymer, so it is not seen in the absorbance, emission, or excitation spectra of the thin films. The initial UV-vis absorbance shows a broad band between 400 and 500 nm characteristic of DE-ANT with a maximum at 451 nm. The initial emission spectrum is dominated by a maximum acene peak at 536 nm for 5%, 554 nm for 10%, and 570 nm for 20% DE-ANT/PMMA thin films. The peaks at 607 nm and 662 nm in the 20% thin film emission spectrum are most likely due to aggregation that resulted from the high acene concentration. Even in the 10% thin film, there is a hint of shoulder that appears around 650 nm which is indicative of aggregation.

The emission maximums of the thin films are all red-shifted from 492 nm, the maximum emission of DE-ANT in dichloromethane and in conjugated polymer nanoparticles. This red-shifting was due to either exciton trapping by the more rigid thin-film matrix or acene aggregation effects.[11,13] The emission maximum blue-shifts as the acene doping percentage decreases. Blue-shifting of the maximum emission also occurs over the course of the irradiation supports the theory that as acene is oxidized, aggregation is broken up and exciton trapping is interrupted by the addition of $^1O_2$ (see SI).

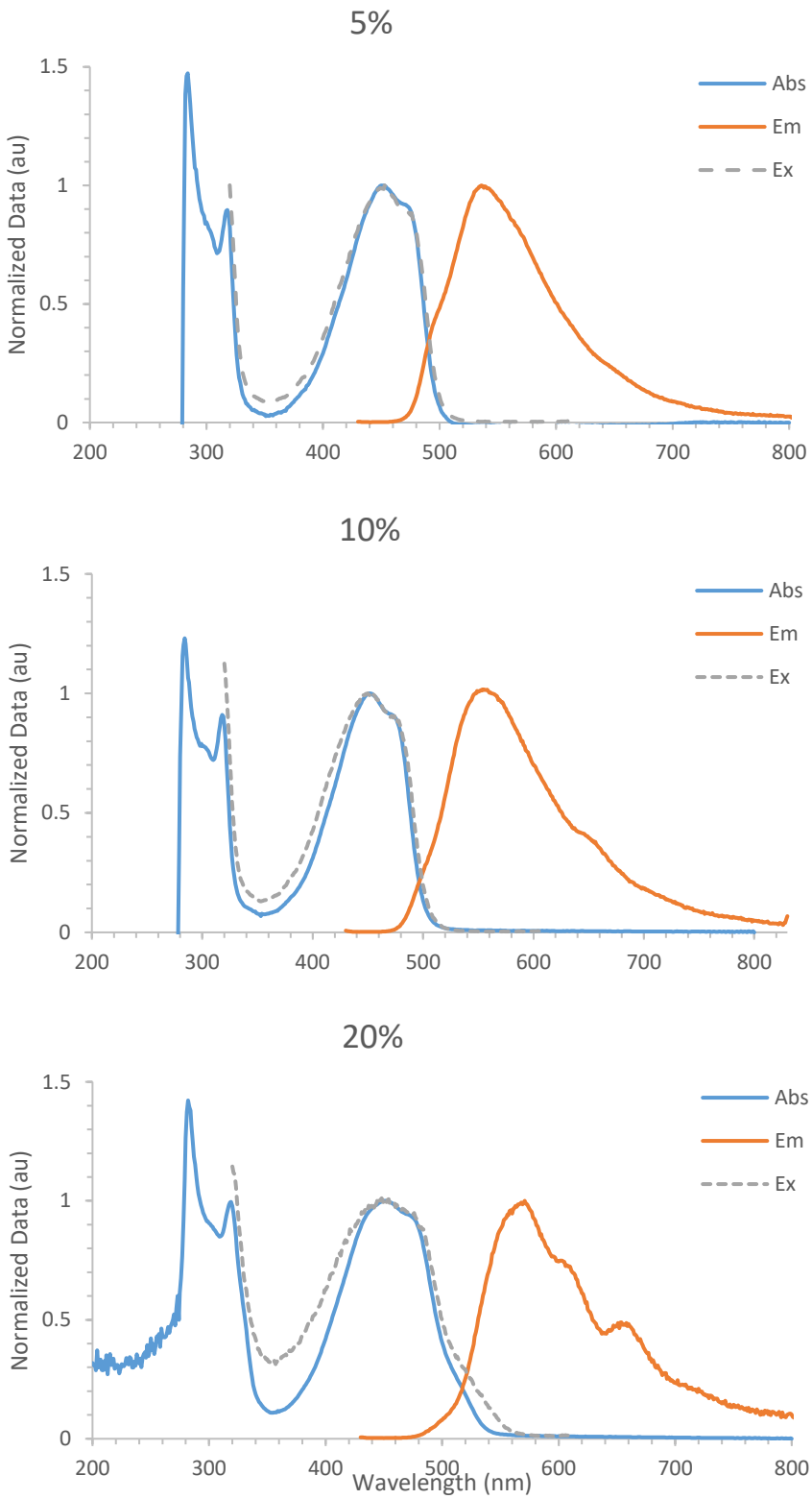

Figure 8. Normalized UV-vis absorbance (left, blue), excitation (left, gray), and emission (right, orange) of DE-ANT/PMMA thin films spun at 1000 rpm. [YZ2]

For the 5% and 10% thin films, the following experiments were conducted by using cycles of (a) irradiation and no heat, or (b) irradiation and heat in an 80°C variac oven. Negative controls were conducted using thin films that underwent (c) no irradiation and no heat, and (d) no irradiation and heat in an 80°C variac oven. The thin films that were not heated were left in the dark at room temperature. Positive control experiments were conducted by irradiating the thin films and allowing it to remain (e) in the dark at room temperature or (f) in an 80°C variac oven. These control experiments were performed to observe and test the conditions necessary for the cycloreversion that is responsible for the endoperoxide produced during irradiation reverting to the parent acene.

The irradiation and cycloreversion of the 5% and 10% thin films were followed by UV-vis absorbance and fluorescence emission spectra. The thin films were irradiated with visible light until the absorbance of DE-ANT reached a plateau. By irradiating the thin films with wavelengths of light absorbed by the acene, we hypothesize the acene will self-sensitize $^1O_2$ from atmospheric O_2 and then undergo [4+2] cycloaddition which will decrease the absorbance of the thin films (Figure 9).

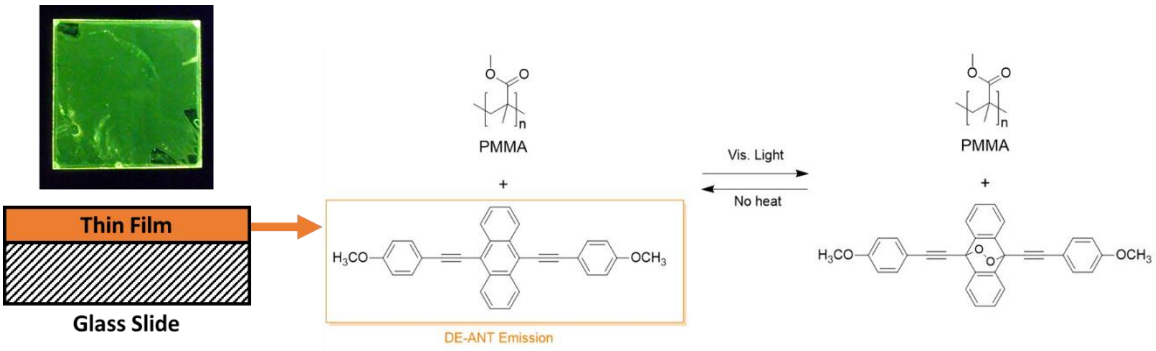

Figure 9. Acene-doped polymer thin films are prepared by spin-casting 0.3 ml of DE-ANT/PMMA in chloroform solution onto glass microscope cover slips. Irradiation with visible light generates $^1O_2$, which reacts with the DE-ANT in the DE-ANT/PMMA thin film.

Films doped at 10% w/w responded to irradiation in 20 min, while those doped at 5% responded the fastest at 10 min. Films with more acene require more irradiation to lower the acene concentration.[17] During the first round of heating, reversion of acene in 5%, 10%, and 20% thin film doping percentages at both room temperature and in the 5% and 10% thin films at 80°C (heating experiments were not conducted on 20% thin films). This reversion can be seen in both the absorbance and emission spectra (see Figure 10 and SI[YZ3]).

All thin films that displayed cycloreversion through an increase in the acene peak absorbance were irradiated again and then allowed to revert again. This time only the thin films that were placed at room temperature reverted (see SI[YZ4]). The absorbance of the thin films heated to 80°C did not change from their absorbance at the end of the second round of irradiation, suggesting the DE-ANT in these thin films had reached the point where they will no longer cyclorevert or thermally decomposed.

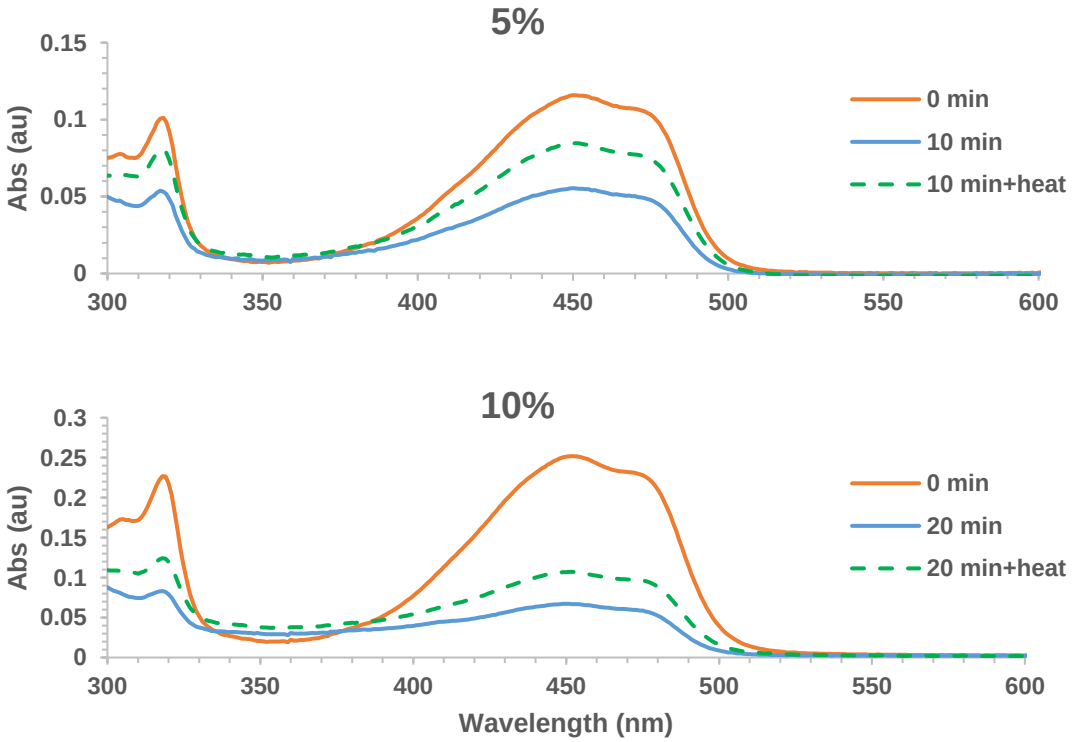

Figure 10a. UV-vis absorbance of 5% and 10% DE-ANT/PMMA thin films before irradiation, at the end of irradiation, and after cycloreversion at 80°C.

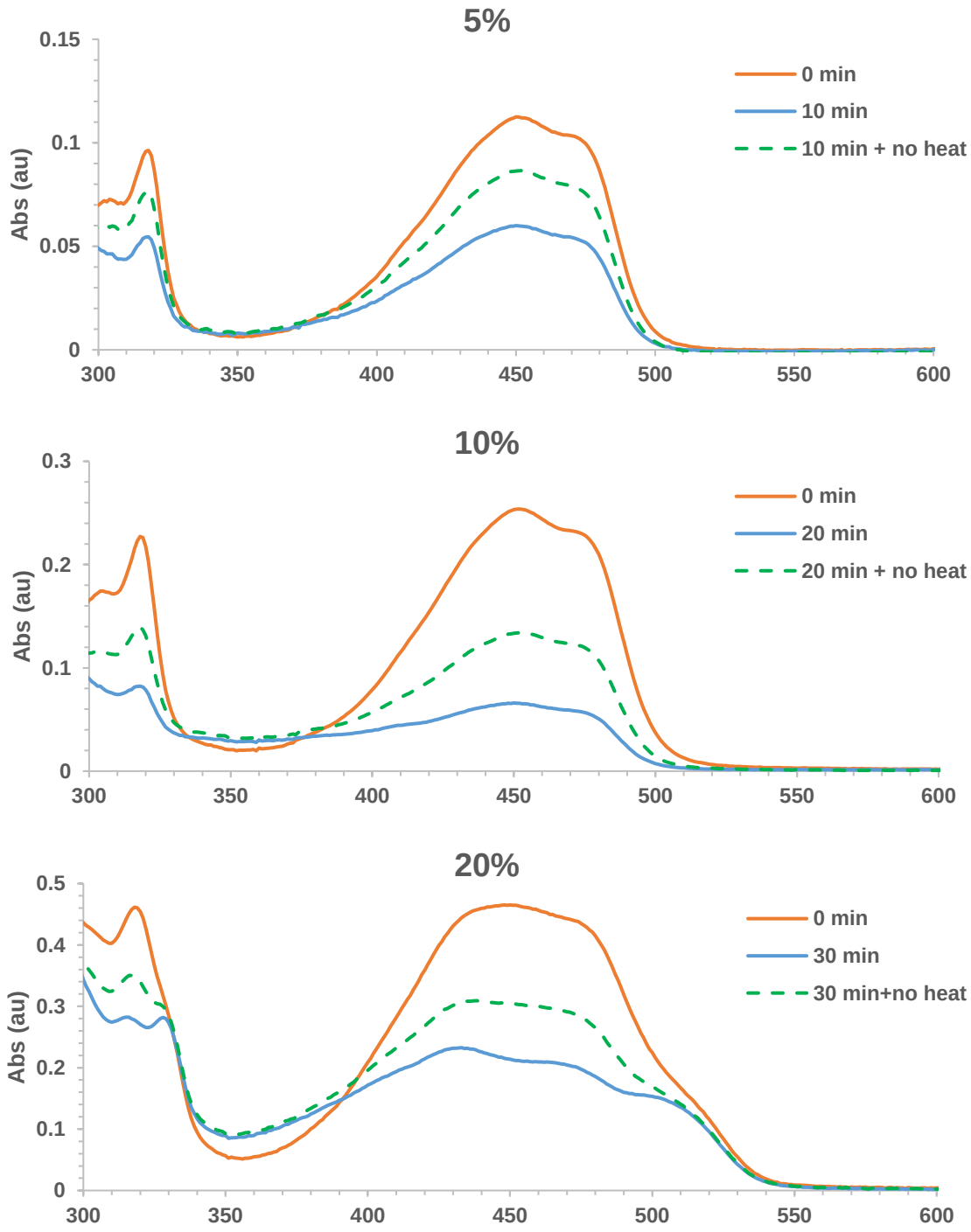

Figure 10b. UV-vis absorbance of 5%, 10%, and 20% DE-ANT/PMMA thin films before irradiation, at the end of irradiation, and after cycloreversion at room temperature.

The percent of acene reverted was calculated by finding the difference between the initial absorbance and the absorbance after heating divided by the difference between the initial absorbance and the absorbance at the end of irradiation.

Eq. 2 $\%\ acene\ reversion = \frac{Abs_{initial} - Abs_{after\ heat}}{Abs_{initial} - Abs_{after\ irradiation}}$

At room temperature, 49.9%, 63.8%, and 59.5% of the DE-ANT endoperoxide generated reverted to the parent acene during the first round of irradiation and heating in the 5%, 10%, and 20% DE-ANT/PMMA thin films respectively. So the 10% DE-ANT/PMMA thin films had the most efficient cycloreversion, none of the thin films regained 100% of the acene. This aligns with the results from the nanoparticles.

Following the first round of irradiation and heating, both the 5% and 10% thin films that were left at room temperature and at 80°C showed a reversion of the acene in the absorbance. So these thin films were irradiated again until the acene peak reached a plateau. This second round of irradiation only took 4 minutes for the 5% and 6 minutes for the 10%.

Two negative control experiments for both the 5% and 10% DE-ANT/PMMA thin films were conducted: (i) allowing a thin film to remain in the dark at room temperature, and (ii) allowing a thin film to remain in the dark in an 80°C variac oven. Both experiments showed no appreciable change in the absorbance spectrum. These results suggest that the thin films are stable are both ambient and temperatures up to 80°C. A positive control experiment for both thin films were conducted by irradiating a thin film and allowing it to remain in the dark at room temperature without undergoing continuous cycles of continuous irradiation and heating. This thin film showed acene reversion in the absorbance spectrum to ~50% of the original absorbance, which suggests room temperature provides enough energy for endoperoxide reversion of DE-ANT when it is trapped in a thin film.

V. Conclusion

By doping DE-ANT into PFO nanoparticles, we have developed a nanoparticle that undergoes a ratiometric fluorescence response during both irradiation and heating. We showed that the endoperoxide formed during irradiation cycloreverts when heated to return to the parent acene in 5%, 10%, and 20% DE-ANT/PFO nanoparticles, but not in the 1%. DE-ANT/PMMA thin films were used to further study the behavior of DE-ANT during continuous cycles of irradiation and heating in an optically clear solid matrix without the photo effects of PFO. Cycloreversion occurred in 5%, 10%, and 20% DE-ANT/PMMA thin films after the first round of irradiation and heating for both the thin films that were heated to 80°C and left at room temperature, but only the room temperature thin films reverted after the second round of irradiation and heating. In both the nanoparticles and thin films DE-ANT endoperoxide only partially reverted, so it is possible that DE-ANT decomposition is occurring in addition to reversion.

The reversibility of singlet oxygen reactions with acene-doped conjugated polymer nanoparticles has important applications for producing reusable oxidation-stable acene-based $^1O_2$ detectors. The tunability of acenes and the wide variety of commercially available conjugated polymers would allow us to optimize the nanoparticle for strong absorption in the red/infrared region of the electromagnetic spectrum, which would allow for deeper tissue penetration, since tissue is much transparent at longer wavelengths. Advancing singlet oxygen generation and detection methods can improve current photodynamic therapies, fluorescence imaging, and tumor detection methods.

VI. Future Directions

While our results are promising, more work needs to be done to optimize the reversibility of other acene-doped conjugated polymer systems.

A. DE-TET/PFO Nanoparticles

FRET occurs between two chromophores when an excited donor transfers energy to a ground state acceptor through nonradiative long-range dipole−dipole interactions.[18] The absorbance spectrum of DE-TET and the emission spectrum PFO do not have large spectral overlap. Inefficient FRET is expected, which should yield an emission spectra dominated by both a large PFO peak and a large DE-TET peak. However, if energy transfer from the conjugated polymer to the acene does not occur via the Förster mechanism, the donor/(donor+acceptor) ratio will differ.

B. DE-TET Endoperoxide/PMMA Thin Films

In the DE-ANT/PMMA thin films, DE-ANT is irradiated to self-sensitize $^1O_2$ and react with $^1O_2$ to form an endoperoxide. The percentage of acene that is actually converted to endoperoxide is unknown, so by making an endoperoxide doped thin film, we can observe the reversion of a thin film known to contain endoperoxide. DE-TET endoperoxide has a longer lifetime than DE-ANT endoperoxide and can be generated by selectively irradiating methylene blue in a DE-TET/$CHCl_3$ solution, which makes it ideal for this experiment.

VII. References

1. DeRosa, M.C. and Crutchley, R.J. Photosensitized singlet oxygen and its applications. *Coordination Chemistry Reviews*. **2002.** 351-371
2. P. R. Ogilby, Chem. Soc. Rev. 2010, 39, 3181–3209.
3. Y. You, W. Nam, Chem. Sci. 2014, 5, 4123–4135.
4. K. Tanaka, T. Miura, N. Umezawa, Y. Urano, K. Kikuchi, T. Higuchi, T. Nagano, J. Am. Chem. Soc. 2001, 123, 2530– 2536.
5. N. Umezawa, K. Tanaka, Y. Urano, K. Kikuchi, T. Higuchi, T. Nagano, Angew. Chem. Int. Ed. 1999, 38, 2899–2901.
6. S. K. Pedersen, J. Holmehave, F. H. Blaikie, A. Gollmer, T. Breitenbach, H. H. Jensen, P. R. Ogilby, J. Org. Chem. 2014, 79, 3079–3087. 21 S. Kim, T. Tachikawa, M. Fujitsuka, T. Majima, J. Am. Chem. Soc. 2014, 136, 11707–11715.
7. Kim, S.; Fujitsuka, M.; Majima, T. *The Journal of Physical Chemistry B.* **2013,** *117* (45), 13985–13992.
8. Zhang, J.; Sarrafpour, S.; Pawle, R. H.; Iii, S. W. T. *Chemical Communications* **2011**, *47* (12), 3445.
9. Altinok, E.; Frausto, F.; Thomas, S. W. Water-soluble fluorescent polymers that respond to singlet oxygen. *Journal of Polymer Science Part A: Polymer Chemistry* **2016**, *54*, 2526-2535.
10. Fudickar, W.; Linker, T. Why Triple Bonds Protect Acenes from Oxidation and Decomposition. *J. Am. Chem. Soc.*, **2012**, *134*, 15071–15082.
11. Zhang, J.; Smith, Z. C.; Thomas, S. W. III "Electronic Effects of Ring Fusion and Alkyne Substitution on Acene Properties and Reactivity" *J. Org. Chem.* **2014**, *79*, 10081–10093.
12. Wu, C.; Bull, B.; Szymanski, C.; Christensen, K.; Mcneill, J. *ACS Nano* **2008**, *2* (11), 2415–2423.
13. Wu, C.; Mcneill, J. Langmuir 2008, 24 (11), 5855–5861.
14. Liou G.Y., Storz P. Reactive oxygen species in cancer. *Free radical research*. **2010**, *44*, 1-31.
15. Josefsen LB, Boyle RW. Photodynamic Therapy and the Development of Metal-Based Photosensitisers. *Metal-Based Drugs*. **2008**, 276109.
16. Sirtonski, M. R.; Mcfarlane, S. L.; Veinot, J. G. C. *Journal of Materials Chemistry* **2010**, *20* (37), 8147.
17. Koylu, D.*; Sarrafpour, S.*; Zhang, J.; Ramjattan, S.; Panzer, M. J.; Thomas, S. W., III "Acene-Doped Conjugated Polymer Films for Singlet Oxygen Dosimetry and Biosensing" *Chem. Commun.* **2012,** *48*, 9489–9491.
18. Wu, M.; Xu, X.; Wang, J.; Li, L. *ACS Applied Materials & Interfaces* **2015,** *7* (15), 8243–8250.
19. Fudickar, W.; Linker, T. *Chemistry - A European Journal* **2011,** *17* (49), 13661–13664.

VIII. Supporting Information

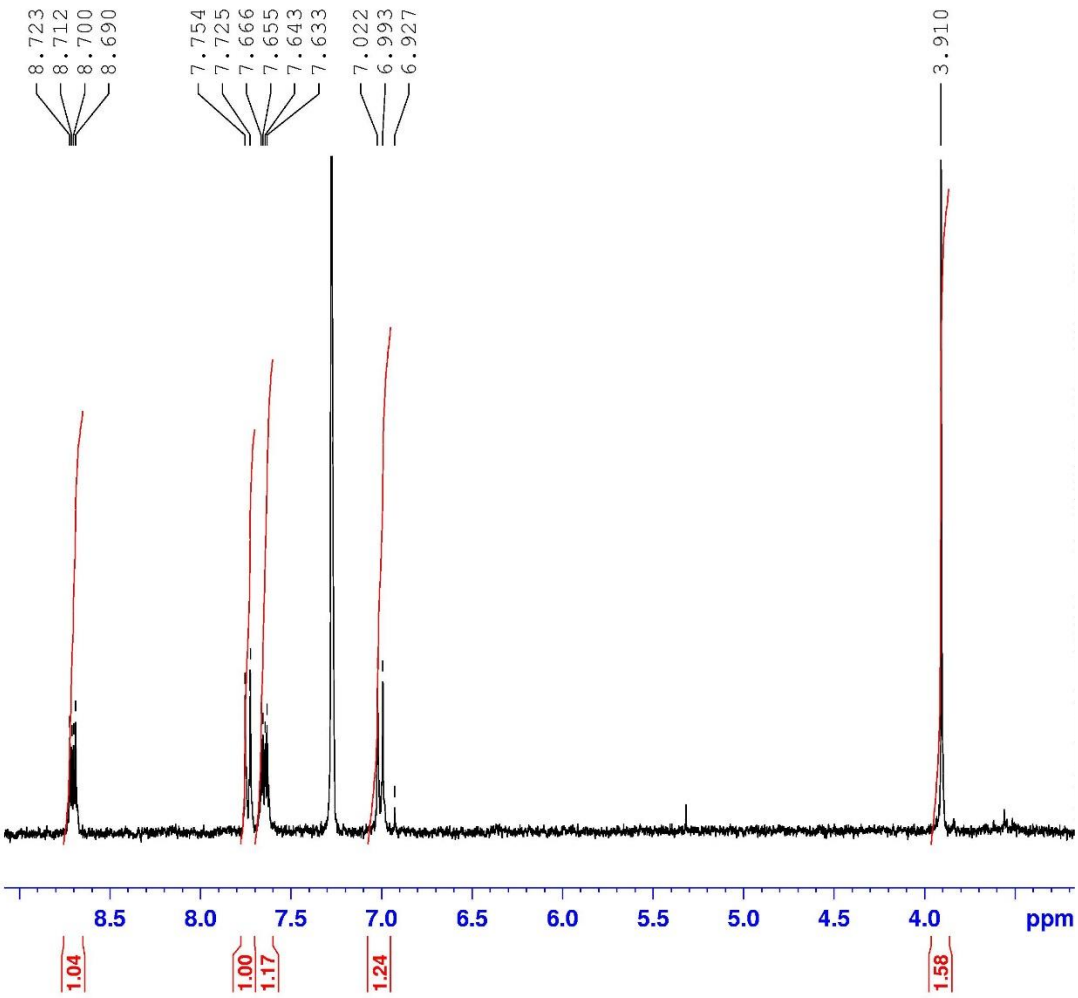

Figure S1. ^{1}H NMR of DE-ANT in $CDCl_3$.

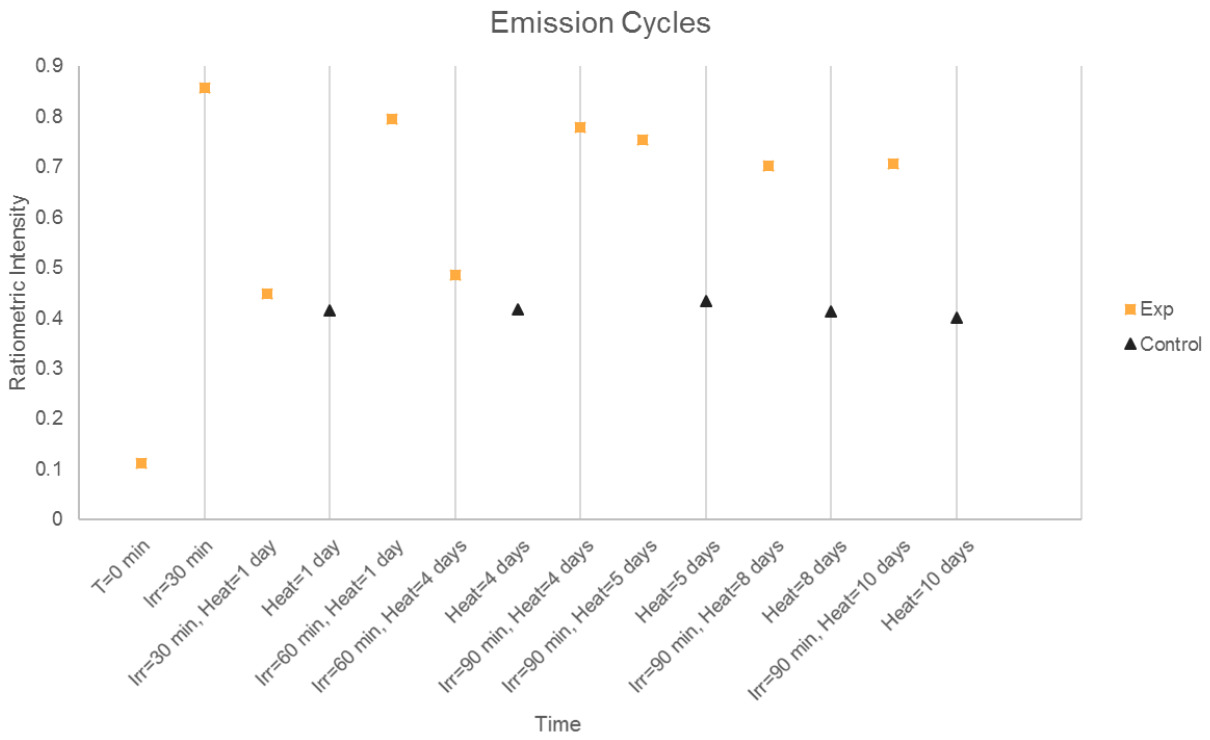

Figure S2. Prolonged heating causes the donor/(donor+acceptor) ratio to increase from 0.11 until the ratio stabilizes after one day of heating at 0.42±0.01. 10% DE-ANT/PFO nanoparticles made using PFO from Sigma Aldrich were used to obtain this data.

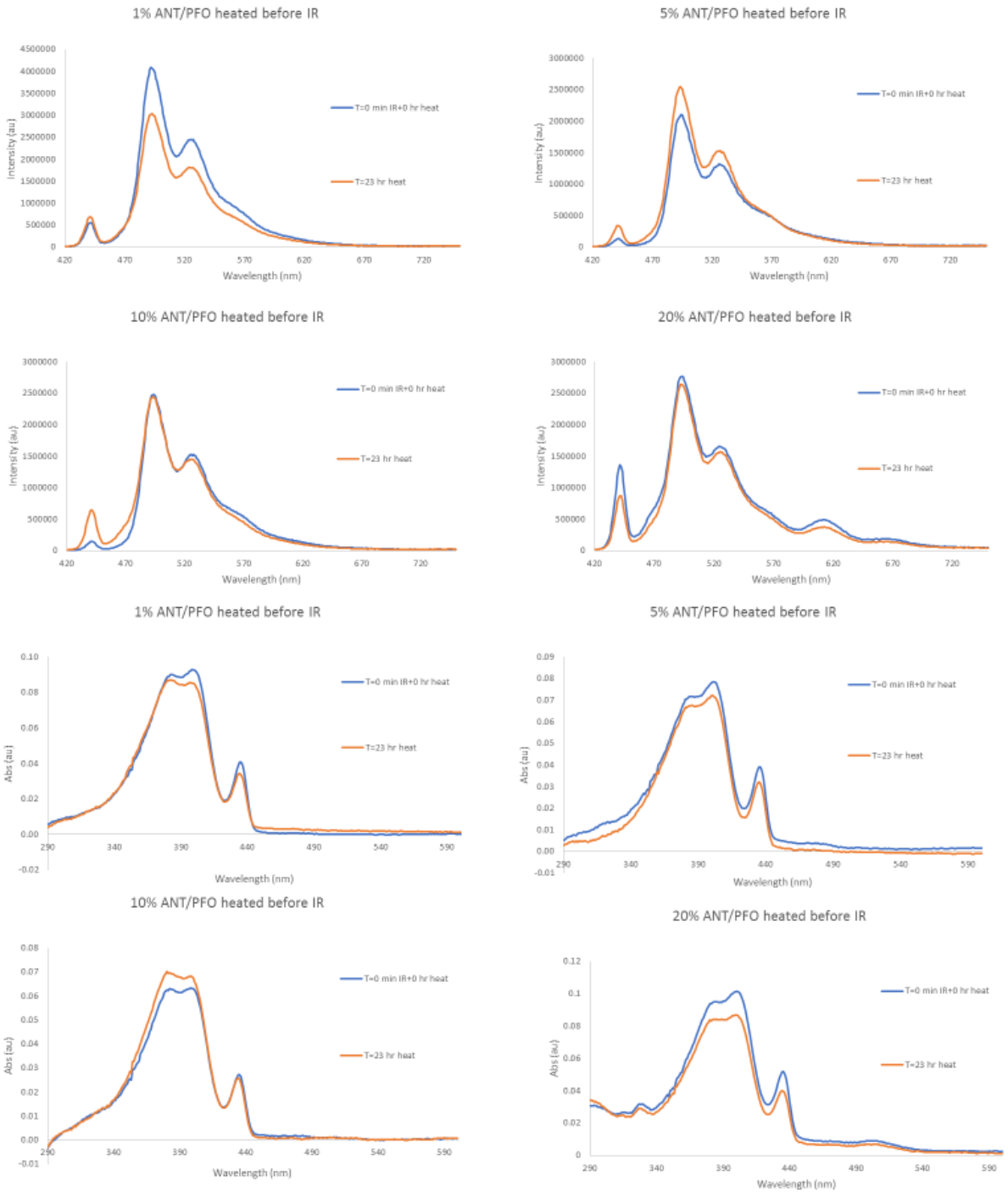

Figure S3. Emission and UV-vis spectra of 1%, 5%, 10%, and 20% DE-ANT/PFO nanoparticles after heat stabilization.

Figure S4. Emission and UV-vis spectra of 1%, 5%, 10%, and 20% DE-ANT/PFO nanoparticles during the first irradiation.

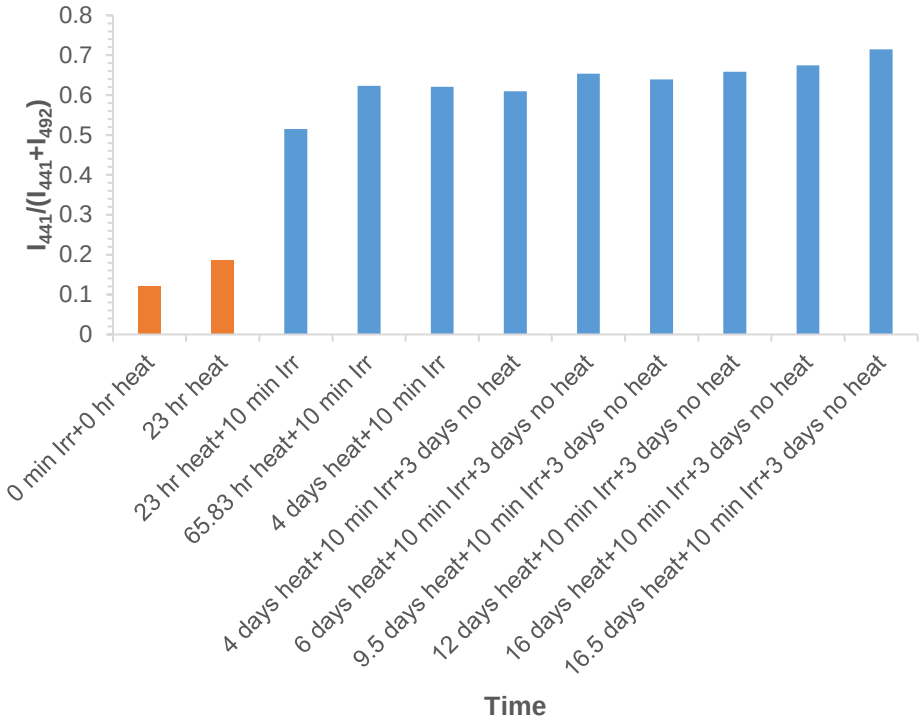

Figure S5 (a). Donor/(donor+acceptor) ratios of heat-stabilized 5% DE-ANT/PFO nanoparticles during repeated cycles of irradiation and heating.

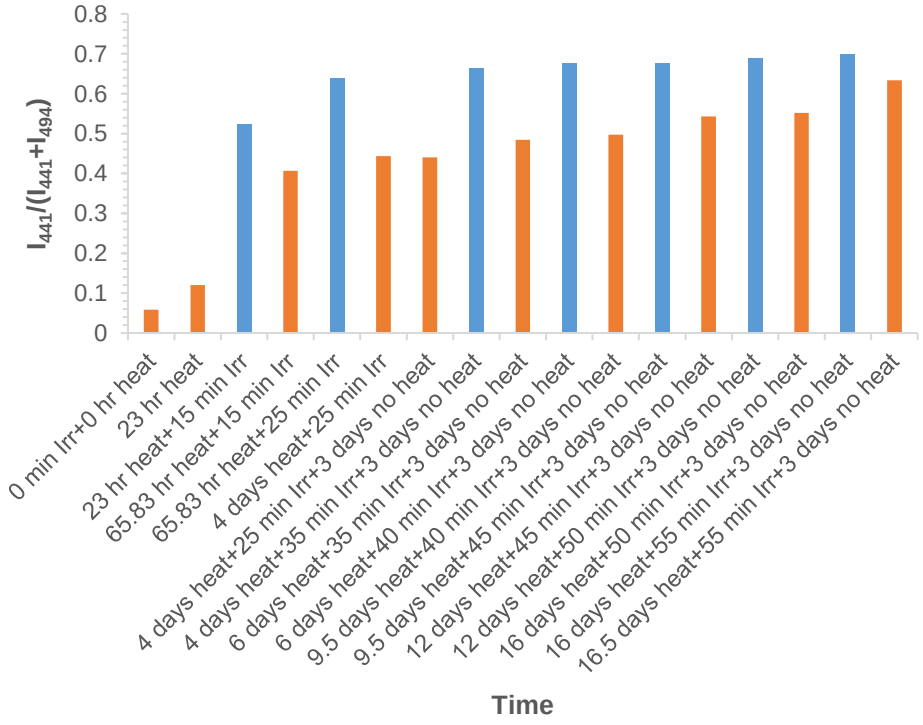

Figure S5 (b). Donor/(donor+acceptor) ratios of heat-stabilized 5% DE-ANT/PFO nanoparticles during repeated cycles of irradiation and heating.

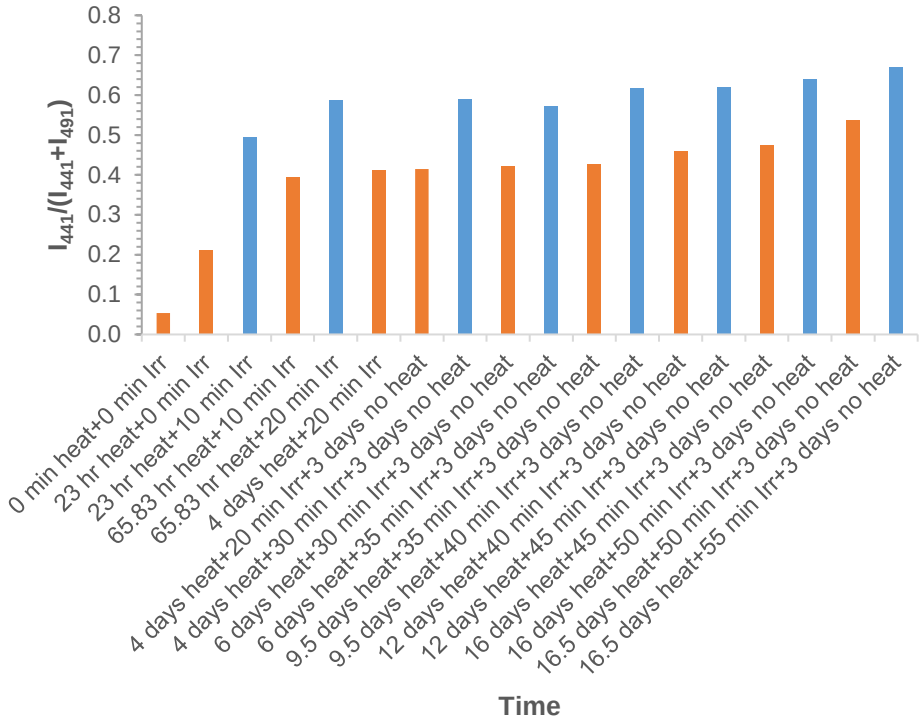

Figure S5 (c). Donor/(donor+acceptor) ratios of heat-stabilized 10% DE-ANT/PFO nanoparticles during repeated cycles of irradiation and heating.

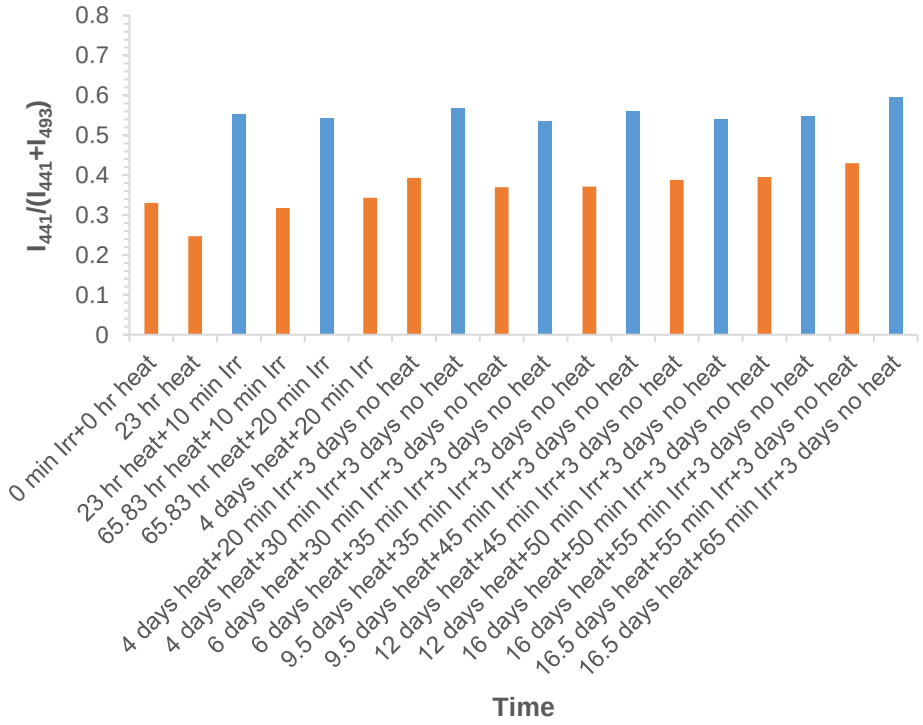

Figure S5 (d). Donor/(donor+acceptor) ratios of heat-stabilized 20% DE-ANT/PFO nanoparticles during repeated cycles of irradiation and heating.

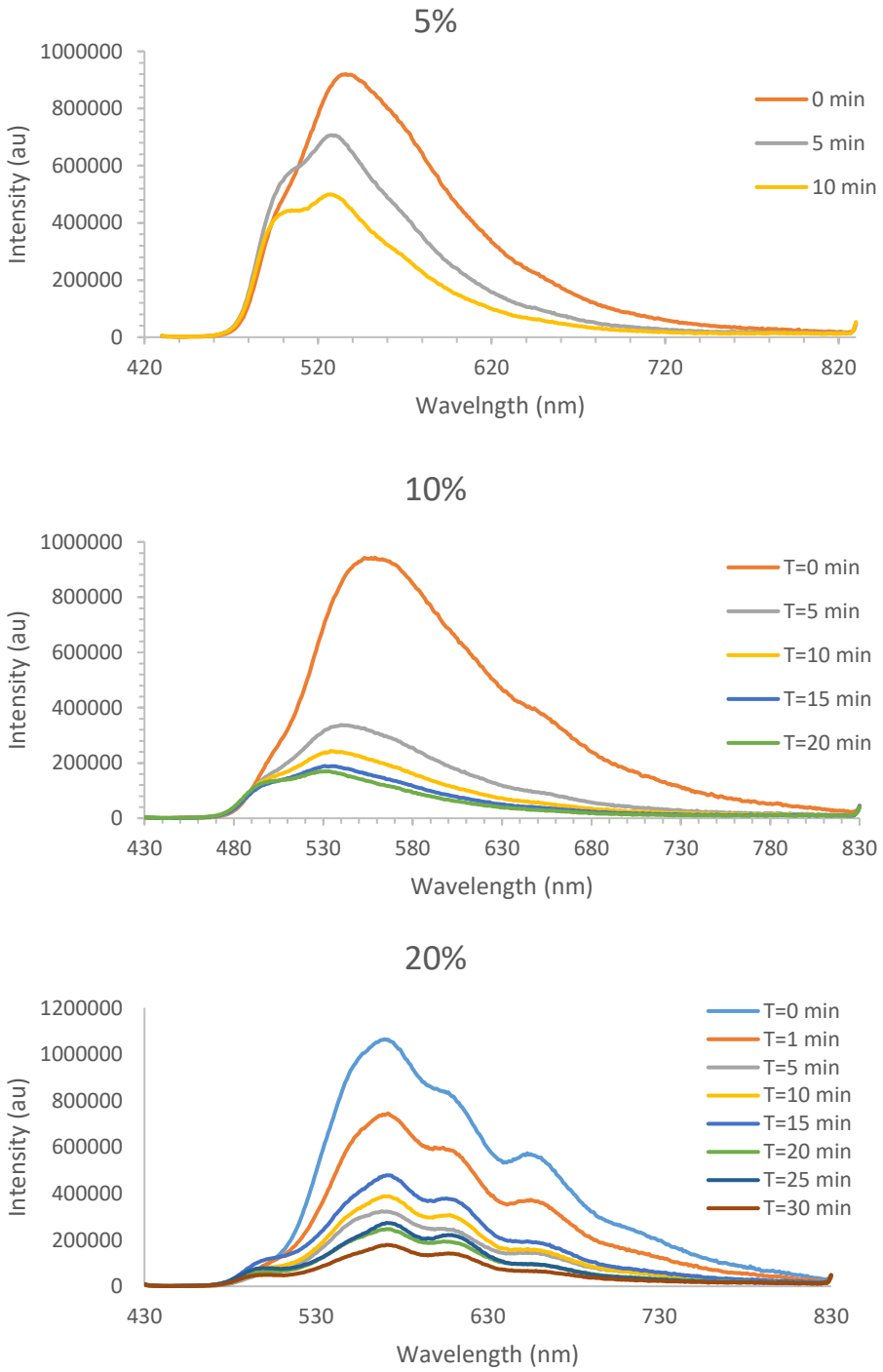

Figure S6. Emission spectra of DE-ANT/PMMA thin films spun at 1000 rpm during irradiation with unfocused visible light.

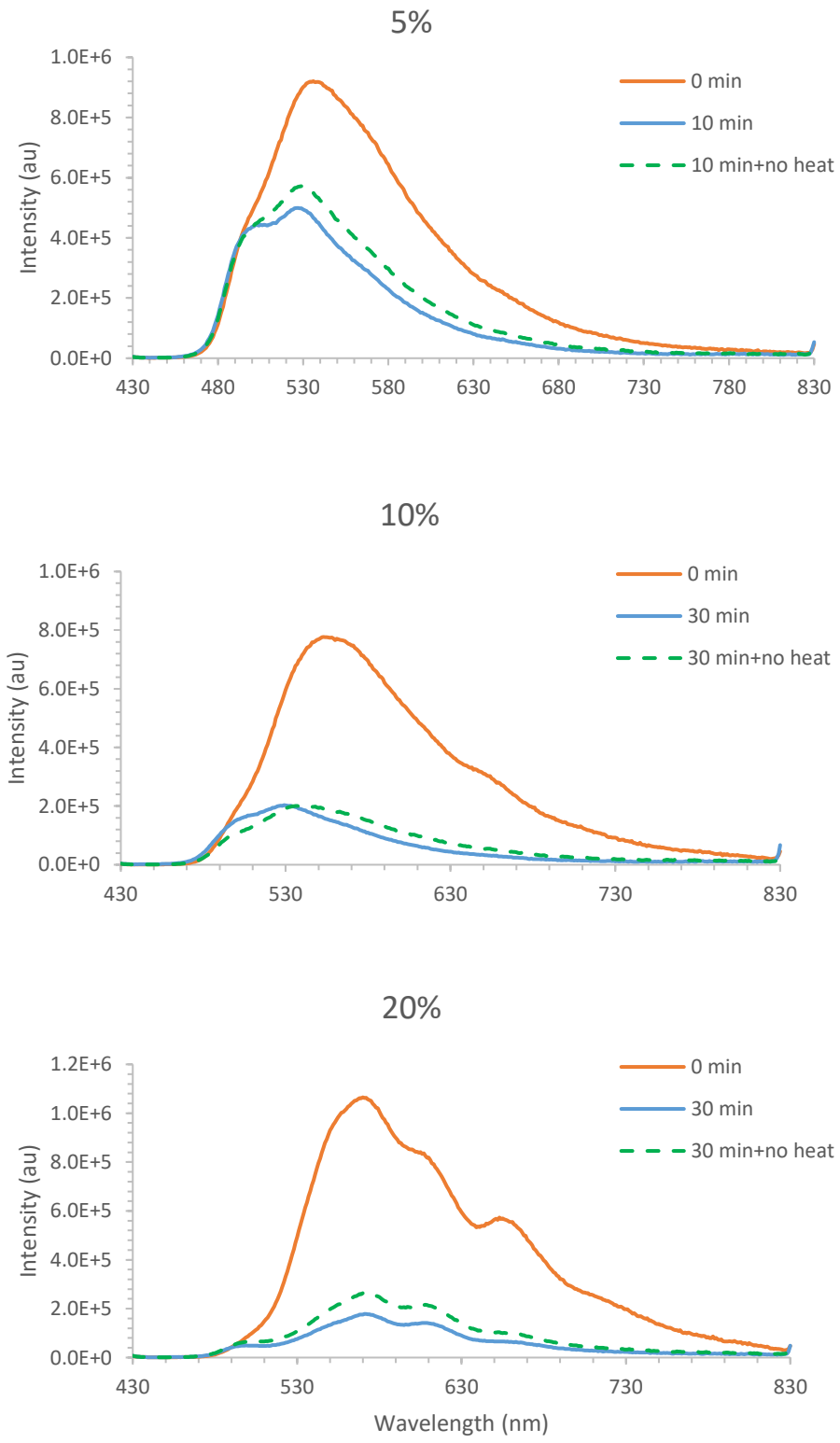

Figure S7. 5%, 10%, and 20% DE-ANT/PMMA thin films before irradiation, at the end of irradiation, and after cycloreversion at room temperature.

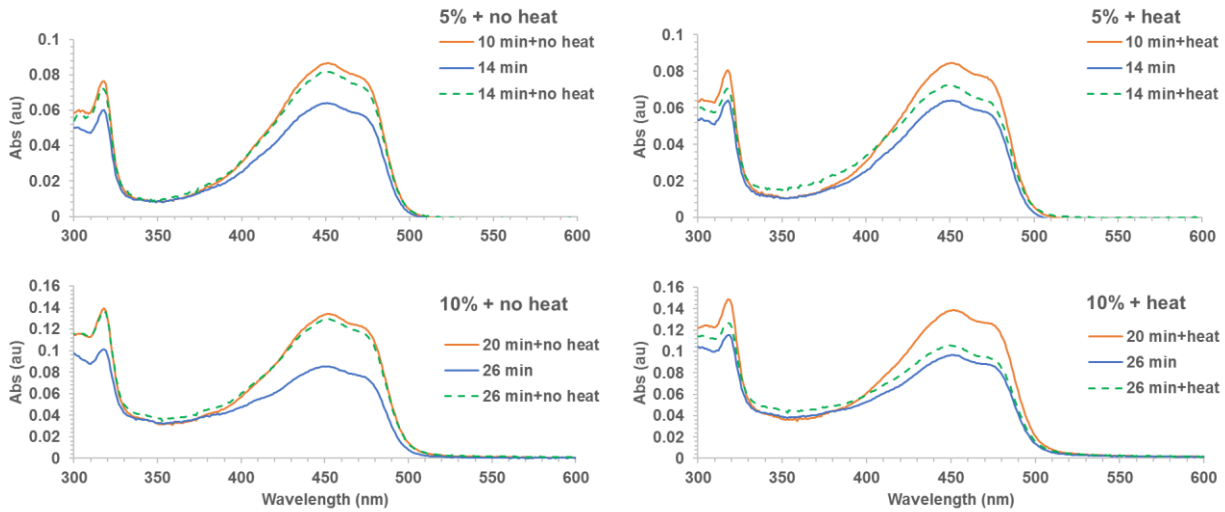

Figure S8. UV-vis absorbance of 5% and 10% DE-ANT/PMMA thin films before second irradiation, at the end of second irradiation, and after second cycloreversion at room temperature (left) and 80°C (right).